Anodic performance in lithium-ion batteries of graphite-like materials prepared from anthracites and unburned carbon concentrates from coal combustion fly ashes

Comportamiento como ánodos en baterías de ión-litio de materiales grafíticos preparados a partir de antracitas y concentrados de inquemados de cenizas volantes procedentes de la combustión de carbón

I. Cameán*, A. B. García, A. Ramos, N. Cuesta

Instituto Nacional del Carbón, CSIC, Francisco Pintado Fe 26, 33011-Oviedo, Spain

**Corresponding author: icamean@incar.csic.es*

Abstract

The electrochemical performance as anodes for lithium-ion batteries of graphite-like materials that were prepared from anthracites and unburned carbon concentrates from coal combustion fly ashes by high temperature treatment was investigated by galvanostatic cycling of lithium test cells. Some of the materials prepared have provided reversible capacities up to ~ 310 mA h g^{-1} after 50 discharge/charge cycles. These values are similar to those of oil-derived graphite (petroleum coke being the main precursor) which is currently used as anodic material in commercial lithium-ion batteries. Larger reversible lithium storage capacities were obtained by using those materials with higher degree of graphitic structural order as evaluated from X-ray diffraction and Raman spectroscopy. In this context, reasonably good linear correlations between the battery reversible capacity and the structural parameters of the electrode-forming materials were found. Furthermore, all materials prepared showed excellent retention of the charge capacity along the cycling as well as low values of the irreversible capacity. Apparently, both the high degree of structural order and the irregular morphology of the particles appear to contribute to the good electrochemical performance as anode in lithium-ion batteries of these materials, thus making feasible their utilization to this application.

Resumen

En este trabajo se ha estudiado la aplicación como ánodos en baterías de ión-litio de materiales grafíticos que habían sido previamente preparados mediante tratamiento térmico a alta temperatura de antracitas y concentrados de inquemados de cenizas volantes procedentes de la combustión de carbón; para ello, se llevaron a cabo ciclados galvanostáticos de baterías de litio tipo test. Algunos de los materiales preparados proporcionaron capacidades reversibles de ~ 310 mA h g^{-1} después de 50 ciclos, siendo estos valores comparables a los correspondientes a grafitos sintéticos (preparados principalmente a partir de coque de petróleo) que en la actualidad son utilizados como ánodo en baterías de ión-litio comerciales. Los valores máximos de capacidad reversible fueron obtenidos para aquellos materiales con mayor grado de orden estructural, el cual ha sido evaluado mediante Difracción de Rayos-X y Espectroscopía Raman. En este sentido, se calcularon correlaciones lineales razonablemente buenas entre la capacidad reversible y los parámetros estructurales de los materiales grafíticos. Además, todos los materiales preparados mostraron excelentes retenciones de la capacidad de carga a lo largo del ciclado, así como valores de capacidad irreversible mínimos. Otros factores no estructurales, tales como la morfología irregular de las partículas de estos materiales también influyeron muy positivamente en las prestaciones de

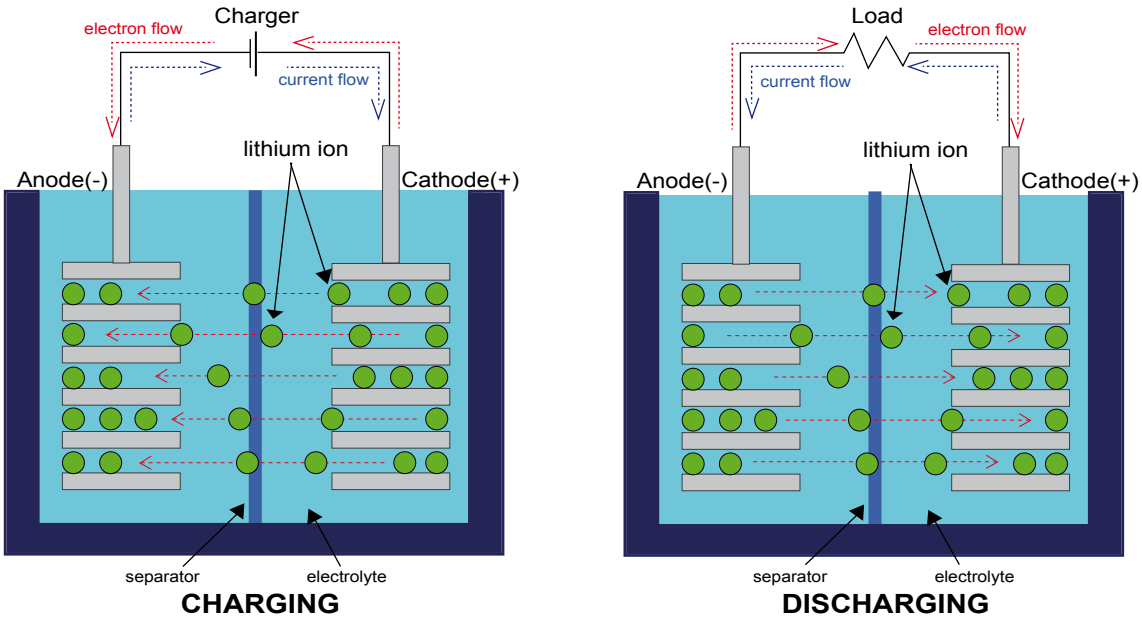

Figure 1. Lithium-ion cell performance: charging and discharging.

Figura 1. Funcionamiento de una celda de ión-litio: carga y descarga.

los ánodos de las baterías, por lo que su utilización para esta aplicación, parece, en principio, factible.

1. Introduction.

Lithium-ion batteries (LIBs) are currently the energy source for most of the portable electronic gadgets such as cellular phones, laptops, digital cameras, work tools, etc. In 2012, the world market of LIBs reached a value of $11.7 \cdot 10^9$ $ USA which can explain the interest, both scientific and technologic, in this kind of batteries. The performance of LIBs is based on the use of intercalation materials as electrodes. During the charge, the lithium ions are de-intercalated from the cathode, they move through the electrolyte and, finally, they are intercalated in the anode. In the discharge, the opposite process occurs spontaneously. The compensation of the charge goes through an external electrical circuit (Figure 1).

Generally, commercially available LIBs use lithium mixed oxides (mainly $LiCoO_2$), solutions of lithium salts in organic solvents and synthetic graphite as cathode, electrolyte and anode, respectively. The choice of graphite as anode is due to its relatively high specific capacity, high cycling efficiency and low irreversible capacity [1-4]. Currently, petroleum coke is the main precursor material in the manufacturing of synthetic graphite [5]. However, it presents the inconvenience of being obtained from an energy source whose reserves are limited. Moreover, a large amount of them are located in countries having serious social and political problems, even immersed in wars. Therefore, other alternative precursors such as coal and coal-derived products have been investigated [6-17]. Among the different classes of coals, anthracites were found to graphitize at temperatures above 2000 ºC [6,8,10]. In this context, graphite with structural characteristics comparable to those of commercially available oil-derived synthetic graphite was prepared from anthracites and unburned carbon concentrates from coal combustion fly ashes by high temperature treatment [11, 12,14-17].

This work is focused on the electrochemical performance as negative electrode in lithium-ion batteries of synthetic graphite that were prepared by high temperature treatment (HTT) of Spanish anthracites and unburned carbon concentrates (UCCs) from coal combustion fly ashes. Specifically, two anthracites denoted AF (91.00 of C wt.%, daf basis) and ATO (93.13 of C wt.%, daf basis), from Villablino in the north-west of Spain were selected for this study. A representative sample of both anthracites was ground to size < 20 μm for the heat treatment experiments. On the other hand, three UCCs that were obtained from A or B pulverized coal combustion fly ashes (mainly fed with anthracites) by screening out the ≤ 80 μm fraction (A/CVP) and following an oil agglomeration methodology described previously [18] by using a waste vegetable oil at concentrations of 1 wt.% (B/CIQ1) and 5 wt.% (B/CIQ5) were also heat treated. Unburned carbon contents of 54.64, 78.35 and 68.02 wt.% were determined for A/CVP, B/CIQ1 and B/CIQ5, respectively. The HTT of the anthracites and UCCs were carried out at the temperature interval of 1800-2800 ºC in a graphite electrical furnace for 1 h under argon flow. The heating rates were 25, 20 and 10 ºC min^{-1} in the ranges: room temperature-1000 ºC, 1000-2000 ºC and 2000-prescribed temperature, respectively. The materials thus prepared were identified by the precursor and the treatment temperature such as ATO/2600 and B/CIQ5/2400.

2. Structural characteristics of the graphite-like materials prepared from anthracites and unburned carbon concentrates from coal combustion fly ashes.

All materials prepared were characterized by means of X-ray diffraction (XRD), and Raman spectroscopy following the methodology previously described in other works [12,14,15,19]. For comparative purposes, a petroleum-based graphite, named SG, was also characterized, this carbon material being commercialized to be employed as anode in the manufacturing of lithium-ion batteries.

The mean interlayer spacing, d_{002}, and crystallite sizes, L_c and L_a, and the relative intensity of the Raman D-band (I_D/I_t where $I_t = I_G + I_D + I_{D'}$) of the materials that were prepared from the anthracites (AF and ATO), and the UCCs (A/CVP, B/CIQ1 and B/CIQ5) by HTT (1800-2800 ºC) are summarized in Table 1. Data corresponding to SG synthetic graphite are also reported.

Table 1. d_{002}, L_c, L_a, and I_D/I_t parameters of the materials prepared from ATO and AF anthracites, A/CVP, B/CIQ1 and B/CIQ5 UCCs by HTT and of SG synthetic graphite of reference.

Tabla 1. Parámetros d_{002}, L_c, L_a, y I_D/I_t de los materiales preparados a partir de las antracitas ATO y AF, y los concentrados de inquemados A/CVP, B/CIQ1 y B/CIQ5 mediante HTT, y del grafito sintético de referencia SG.

Material	d_{002} (nm)	L_c (nm)	L_a (nm)	I_D/I_t (%)
ATO/2400	0.3412	8.0	21.2	29.7
ATO/2500	0.3403	9.3	25.7	28.0
ATO/2600	0.3402	9.5	27.6	28.1
ATO/2700	0.3393	11.2	34.1	22.1
ATO/2800	0.3387	12.8	39.1	23.9
AF/2400	0.3382	14.1	44.6	16.5
AF/2500	0.3382	14.6	42.0	18.9
AF/2600	0.3373	18.8	46.7	17.7
AF/2700	0.3370	21.1	49.2	14.2
AF/2800	0.3369	21.6	48.7	12.4
A/CVP/1800	0.3419	7.5	-	45.1
A/CVP/2000	0.3412	8.5	-	34.3
A/CVP/2200	0.3390	12.6	-	22.9
A/CVP/2300	0.3378	18.7	-	16.9
A/CVP/2500	0.3372	26.7	52.5	16.0
A/CVP/2600	0.3368	31.0	53.2	12.5
A/CVP/2700	0.3370	27.5	51.2	12.1
B/CIQ1/2000	0.3420	8.8	21.7	42.6
B/CIQ1/2300	0.3389	16.7	44.5	19.4
B/CIQ1/2500	0.3381	20.1	46.9	16.7
B/CIQ1/2600	0.3377	22.6	46.6	15.4
B/CIQ5/1800	0.3420	7.8	-	53.0
B/CIQ5/2000	0.3410	9.3	-	33.9
B/CIQ5/2200	0.3397	11.5	45.9	19.7
B/CIQ5/2300	0.3384	16.7	51.9	17.3
B/CIQ5/2400	0.3382	18.3	50.3	15.9
B/CIQ5/2500	0.3375	23.0	51.2	14.7
B/CIQ5/2600	0.3373	24.8	51.2	14.8
SG	0.3361	50.4	61.1	9.98

The materials structural data shows that, as the treatment temperature of the precursor is rising, d_{002}, and I_D/I_t decrease whereas the crystallites sizes, L_c and L_a, grow gradually. These facts are associated with the improvement of the degrees of the structural order and crystalline orientation as well as the removal of the surface defects of the materials as a consequence of the development of a three-dimensional graphite structure [6-17]. Furthermore, a comparative analysis of these results leads to the conclusion that the degree of crystallinity of the

materials depends on the precursor. For example, materials with interlayer spacing of 0.3387 nm and 0.3370 nm were prepared from ATO and AF anthracites, respectively, by heating at 2800 ºC (Table 1). This significant difference in the ability to graphitize of both the anthracites and the UCCs has been previously discussed attending to their characteristics (composition, microstructure, mineral matter/ash contents) [6,10,12,15]. Among them, the mineral matter was found to act as a graphitization catalyst, thus explaining the more graphite-like materials obtained from AF anthracite as compared to ATO anthracite, or from A/CVP as compared to B/CIQ1 and B/CIQ5 (see ash contents of the precursors in Table 2).

Table 2. Ash contents of ATO, AF, A/CVP, B/CIQ1 and B/CIQ5.

Tabla 2. Contenido en cenizas de ATO, AF, A/CVP, B/CIQ1 y B/CIQ5.

Material	Ash (wt.%, dry basis)
AF	10.12
ATO	19.74
A/CVP	45.36
B/CIQ1	21.65
B/CIQ5	31.98

According to a mechanism proposed for the catalytic graphitization of hard carbons [20], the active constituents of the mineral matter of the carbon material (Al, Fe, Si, etc) would preferentially react with disordered carbons located in the edges of the turbostratic domains to form the corresponding carbide. Subsequently, this carbide would decompose in graphitic carbon at high temperature by which the size of the already-existing graphite layers would be increased. Because of this catalytic effect, graphite materials showing structural and textural characteristics comparable to those of the petroleum-based graphite of reference (SG) which is currently used in energy applications were prepared from the anthracites and UCCs studied in this work.

3. Electrochemical performance of the graphite-like materials

The electrochemical study of the materials prepared was carried out using two-electrodes Swagelok-type cells which were assembled in a dry box under argon atmosphere and water and oxygen contents below 1 ppm (Figure 2). Working electrodes (WE) were prepared by mixing the active material and polyvinylidene fluoride (PVDF), which acts as binder, in a proportion of 92:8 wt.%, respectively. All of the active materials were ground to 20 µm top size prior the electrode preparation. This mixture or slurry was deposited on a copper foil of 12 mm diameter by airbrushing and dried at 120 ºC for ~ 24 h. Thus, a thin and uniform surface of slurry coating the copper was obtained. Metallic lithium disc of 12 mm diameter was used as counter-electrode (CE). A 1M $LiPF_6$ (EC:DEC, 1:1, w/w) solution impregnating two separator glass micro-fiber disks acts as electrolyte.

The cells were subjected to galvanostatic cycling in the 2.1-0.003 V vs Li/Li^+ voltage range during 50 cycles at a constant current of C/10 corresponding to attain the theoretical graphite capacity of 372 mA h g^{-1} in 10 h, i.e., to form the LiC_6 intercalation compound, being one lithium ion per six carbon atoms the maximum amount of Li^+ that graphite can be inserted in its bulk [21].

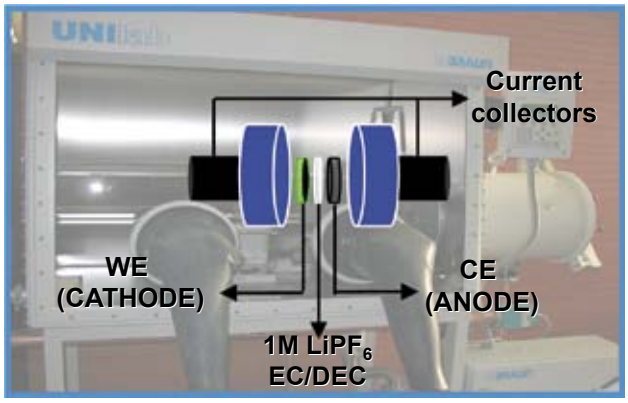

Figure 2. Two-electrode Swagelok-type cell.

Figura 2. Modelo Swagelok de una celda de dos electrodos.

3.1. Lithium intercalation/de-intercalation mechanism

The voltage curves of the first discharge-charge cycle and the second discharge of the lithium cells using A/CVP/2700, B/CIQ5/2600, B/CIQ1/2600, AF/2800 and ATO/02800 as WEs are shown in the Figure 3. For comparison, the voltage profile of the reference graphite, SG, was also included in the same figure. As seen, the mechanism of lithium ions intercalation/de-intercalation in the bulk of these materials is much the same to that of SG. At the beginning of the discharge, the voltage drops quickly to ~ 0.8 V (vs Li/Li^+). At this point, a short *plateau* is observed which is attributed to the electrolyte decomposition causing the formation of solid electrolyte interface (SEI) on the graphite surface and an irreversible consumption of lithium ions [22]. Subsequently, the voltage drops gradually to ~ 0.2 V vs Li/Li^+. Below this point, the lithium intercalation into the material starts as shown by the appearance of three *plateaus* at ~ 0.18 V, ~ 0.10 V and ~ 0.06 V. These plateaus which correspond to the different stages of lithium ions intercalation in graphite-like materials [23] can be better appreciate in the graph insert in Figure 3.

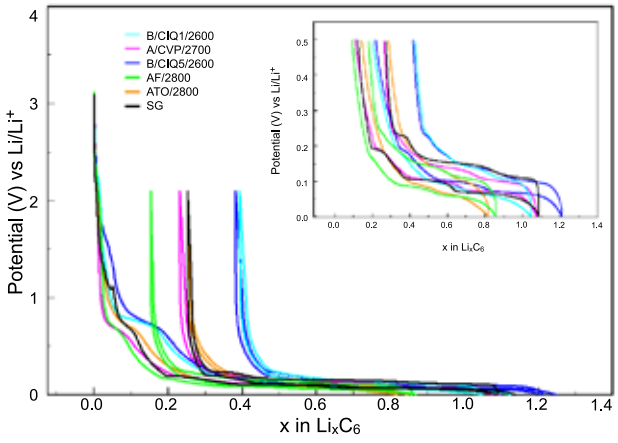

Figure 3. Voltage (V *vs* Li/Li^+) *vs* x in Li_xC_6 during the 1st discharge-charge cycle and 2nd discharge of A/CVP/2700, B/CIQ5/2600, B/CIQ1/2600, AF/2800, ATO/02800 and SG materials.

Figura 3. Voltaje (V *vs* Li/Li^+) *vs* x en Li_xC_6 durante el 1er ciclo de descarga/carga y la 2ª descarga de los materiales A/CVP/2700, B/CIQ5/2600, B/CIQ1/2600, AF/2800, ATO/02800 y SG.

3.2. Reversible capacity and capacity retention along cycling

As an example, the results of the galvanostatic cycling of the graphite-like materials prepared from the UCCs A/CVP and B/CIQ5 together with that of the

SG graphite are presented in the Figure 4 (discharge capacity along cycling plots). Firstly, it is worth to mention that some of the materials prepared in this work, specifically A/CVP/2700 and B/CIQ5/2600, have provided reversible capacities similar to SG graphite (310 mA h g^{-1} after 50 cycles). Furthermore, all of them show a remarkable stable capacity along cycling with capacity keeping values in the range of 90-99 % after 50 cycles. Similar results were attained by cycling the graphite-like materials prepared from AF and ATO anthracites [16].

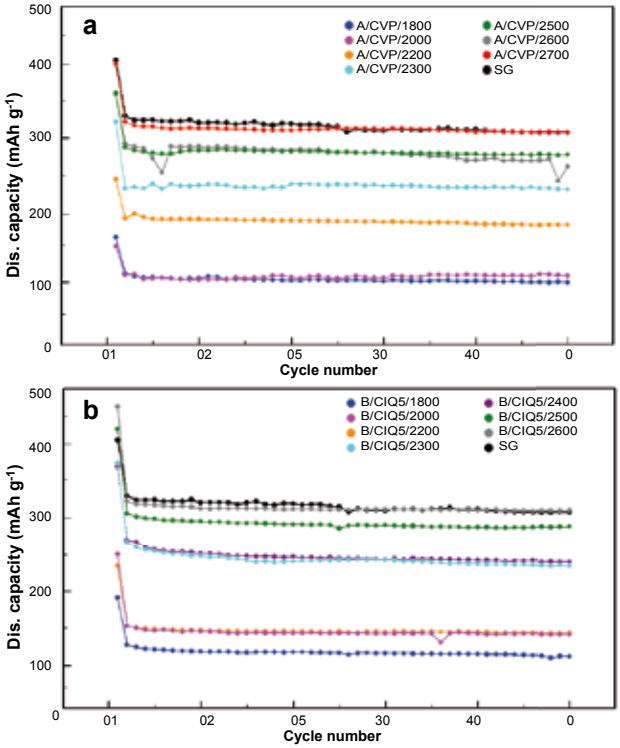

Figure 4. Extended galvanostatic cycling of (a) A/CVP/1800-2700 and SG materials, and (b) B/CIQ5/1800-2600 and SG materials.

Figura 4. Ciclado galvanostático de los materiales: (a) A/CVP/1800-2700 y SG, y (b) B/CIQ5/2600 y SG.

By comparing the galvanostatic cycling results (Figure 4) and the structural parameters (XRD and Raman) of the materials prepared (Table 1), it is clear that those with higher degree of graphitic structural order provide larger lithium storage capacity. For example, battery reversible capacity values of 308 mA h g^{-1} and 185 mA h g^{-1} were measured after 50 cycles by using A/CVP/2700 and A/CVP/2200 materials with crystallite size, L_c, of 28 nm and 13 nm, respectively. In fact, reasonably good linear correlations between the reversible capacity and the structural parameters of the electrode-forming materials were found. For example, R^2 coefficients values of 0.954 and 0.973 were calculated for the interlayer spacing, d_{002}, and the thickness of the crystallite, L_c, of the graphite-like materials obtained from AF and ATO anthracites [16]. The dependence of the electrochemical intercalation of lithium ions in well-ordered carbon materials on their crystal structure has been previously studied by other authors [1,24,25]. The crystal thickness, L_c, was reported to be the most important factor affecting the extent of the reversible capacity provided by a specific material in the electrode. As in the work discussed here, a tendency of the capacity to increase with the material L_c was observed. Nevertheless, no specific correlation between the electrode capacity and the crystal thickness or other crystalline parameters of the materials was established. However, when graphite-like materials of high degree of crystallinity obtained from different precursors were considered, this tendency was not followed at all and larger capacities were delivered by materials with lower or similar L_c values. In this context, as mentioned above, A/CVP/2700 and B/CIQ5/2600 have delivered reversible capacities similar to SG graphite with a much higher L_c crystallite size (Table 1). Therefore, the good electrochemical behaviour of these graphite-like materials that were prepared from the UCCs should be related to other non structural factors. Among them, the influence of the graphite morphology on its electrochemical performance has been widely studied in previous works [1,26-31]. In an attempt to clarify this point, the morphology of A/CVP/2700, B/CIQ5/2600 and SG was studied by SEM and the corresponding micrographs are shown in the Figure 5. SG graphite shows the presence of flakes. Unlike SG, A/CVP/2700 and B/CIQ5/2600 materials have an irregular particle shape which has been suggested to improve the electrode performance due to the formation of voids between particles, thus allowing a good percolation of the electrolyte solution to reach the electrode active mass, i.e., favouring the Li intercalation in the bulk of the graphite-like material [28].

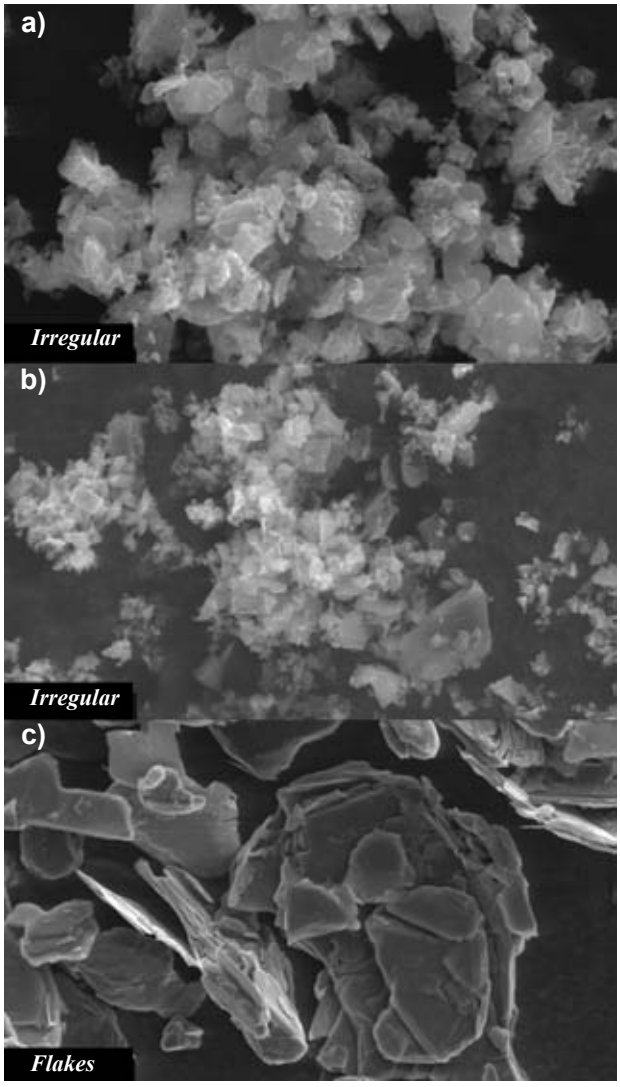

Figure 5. SEM images of a) A/CVP/2700, b) B/CIQ5/2600 and c) SG materials.

Figura 5. Imágenes SEM de los materiales a) A/CVP/2700, b) B/CIQ5/2600 y c) SG.

3.3. Irreversible capacity

The irreversible capacity losses during the first discharge-charge of the graphite-like materials studied are reported in Table 3. Generally, the majority of the materials show irreversible capacity percentages similar to that of SG (~ 25 %). Although other side reactions and phenomena may contribute to the irreversible consumption of lithium ions [32-34], it can be considered that the irreversible capacity is mainly due to the formation of the solid electrolyte interface on the surface of graphite electrode [35]. Because of the SEI film covers the electrode surface exposed to the electrolyte solution it is easy to conclude that irreversible capacity has been related to the surface area of the electrode material [22,32-34,36]. In fact, proportionality with the BET specific surface area was found in graphite materials belonging to the same family. In this work, the values of the BET specific surface area of the graphite-like materials prepared are < 10 m^2 g^{-1}, being the typical values for petroleum-based graphites used as anodes in commercial LIBs [37]. Therefore, as expected, the values of irreversible capacity of these materials and SG are comparable. However, there is no dependence between these two parameters. In previous works, it has been found a relation between the irreversible capacity and the active surface area (ASA) of the carbon materials [33,34]. The ASA is defined as the cumulated area of the different type of defects present on the carbon surface (stacking faults, dislocations and vacancies). Therefore, the ASA can be considered as indirect estimation of the degree of structural order of the material. But any relation has been found between the development of the three-dimensional graphite structure and the BET specific surface area or ASA (indirectly estimated from the structural parameters). Taking into account that no exfoliation has been observed during the first discharge, other factors different than the order and microcrystal orientation should influence on the irreversible charge loss.

Table 3. First cycle irreversible capacity of the materials prepared from ATO and AF anthracites, and A/CVP, B/CIQ1 and B/CIQ5 UCCs by HTT and of the SG synthetic graphite of reference.

Tabla 3. Capacidad irreversible de los materiales preparados a partir de las antracitas ATO y AF, y los concentrados de inquemados A/CVP, B/CIQ1 y B/CIQ5 mediante HTT y el grafito sintético de referencia SG.

Material	C_{irr} (%)	Material	C_{irr} (%)	Material	C_{irr} (%)
ATO/2400	31	A/CVP/1800	37	B/CIQ5/1800	39
ATO/2500	24	A/CVP/2000	31	B/CIQ5/2000	44
ATO/2600	26	A/CVP/2200	25	B/CIQ5/2200	40
ATO/2700	32	A/CVP/2300	24	B/CIQ5/2300	37
ATO/2800	31	A/CVP/2500	21	B/CIQ5/2400	34
AF/2400	27	A/CVP/2600	21	B/CIQ5/2500	31
AF/2500	16	A/CVP/2700	22	B/CIQ5/2600	32
AF/2600	18	B/CIQ1/2000	39	SG	23
AF/2700	20	B/CIQ1/2300	34		
AF/2800	18	B/CIQ1/2500	33		
		B/CIQ1/2600	38		

4. Acknowledgements

Financial support from the Spanish MICINN and MINECO (under Projects MAT2004-01094, ENE2008-06516 and ENE2011-28318) and PCTI of Asturias (under Project PC07-014) is gratefully acknowledged.

5. References

[1] Endo M, Kim C, Nishimura K, Fujino T., Miyashita K. Recent development of carbon materials for Li ion batteries. Carbon 2000; 38:183-197.

[2] Noel M, Sryanarayanan V. Role of carbon host lattices in Li-ion intercalation/de-intercalation processes. J Power Sources 2002; 111:193-209.

[3] Wakihara M. Recent developments in lithium ion batteries. Mater Sci Eng 2001; R33:109-134.

[4] Olson DW. Graphite. In: 2006 Mineral Year Book, U.S. Geological Survey, U.S. Department of Interior, Washington , 2007.

[5] Inagaki M. Applications of polycrystalline graphite. In: Delhaès P, ed. Graphite and precursors. Amsterdam: Gordon and Breach. 2001. p. 179-98.

[6] Oberlin A, Terriere G. Graphitization studies of anthracites by high resolution transmission electron microscopy. Carbon 1975; 13:367-376.

[7] Seehra MS, Pavlovic AS, Babu VS, Zondlo JW, Stansberry PG, Stiller AH. Measurements and control of anisotropy in ten coal-based graphites. Carbon 1994; 32:431-435.

[8] Bustin RM, Rouzaud JN, Ross JV. Natural graphitization of anthracite: experimental considerations. Carbon 1995; 33:679-691.

[9] Kawano Y, Fukuda T, Kawarada T, Mochida I, Korai Y. Puffing behavior during the graphitization of coal-tar-based needle coke impregnated with iron (III) sulfate and boric acid. Carbon 2000; 38:759-765.

[10] Atria JV, Rusinko F, Schobert HH. Structural ordering of Pennsylvania anthracites on heat treatment to 2000-2900 degrees C. Energ Fuel 2002; 16:1343-1347.

[11] González M, Montes-Morán MA, García AB. Graphite materials prepared from an anthracite: A structural characterization. Energ Fuel 2003; 17:1324-1329.

[12] González M, Montes-Morán, MA, Suárez-Ruiz I, García AB. Structural characterization of graphite materials prepared from anthracite of different characteristics: A comparative analysis. Energ Fuel 2004; 18:365-370.

[13] Pappano PJ, Rusinko F, Schobert HH, Struble DP. Dependence of physical properties of isostatically molded graphites on crystallite height. Carbon 2004; 42:3007-3009.

[14] González M, Montes-Morán, MA, García AB. Influence of inherent coal mineral matter on the structural characteristics of graphite materials prepared from anthracites. Energ Fuel 2005, 19:263-269.

[15] Cabielles M, Montes-Morán, MA, García AB. Structural study of graphite materials prepared by HTT of unburned carbon concentrates from coal combustion fly ashes. Energ Fuel 2008, 22:1239-1243.

[16] On the electrochemical performance of anthracite-based graphite materials as anodes in lithium-ion batteries. Fuel 2010; 89:986-991.

[17] Graphite materials prepared by HTT of unburned carbon from coal combustion fly ashes: Performance as anodes in lithium-ion batteries. J Power Sources 2011; 196:4816-4820.

[18] Valdés AF, García AB. On the utilization of waste vegetable oils (WVO) as agglomerants to recover coal from coal fines cleaning wastes (CFCW). Fuel 2006; 85:607-614.

[19] Cameán I. Tesis doctoral. Preparación de materiales grafíticos: Aplicación como ánodos en baterías de ión-litio. Universidad de Oviedo. 2011.

[20] Oberlin A, Rouchy JP. Transformation des carbones non graphitables par traitement thermique en presence de fer. Carbon 1971; 9 :39-46.

[21] Lavela Cabello P, Tirado Coello JL. Baterías de íon-litio. In: Lavela P, Tirado JL, eds. Baterías Avanzadas.

Universidad de Córdoba: Servicio de Publicaciones. 1999. p. 213-246.

[22] Fong R, von Sacken U, Dahn JR. Studies of lithium intercalation into carbons using nonaqueous electrochemical cells. J Electrochem Soc 1990; 137:2009-2013.

[23] Balasooriya NWB, Touzain Ph, Bandaranayake PWSK. Lithium electrochemical intercalation into mechanically and chemically treated Sri Lanka natural graphite. J Phys Chem Solids 2006; 67:1213-1217.

[24] Dahn JR, Sleigh AK, Shi H, Reimers JN, Zhong Q, Way BM. Dependence of the electrochemical intercalation of lithium in carbons on the crystal structure of the carbon. Electrochim Acta 1993; 38:1179-1191.

[25] Endo M, Nishimura Y, Takahashi T, Takeuchi K, Dresselhaus MS. Lithium storage behaviour for various kinds of carbon anodes in Li ion secondary battery. J Phys Chem Solids 1996; 57:725-728.

[26] Arrebola JC, Caballero A, Hernán L, Morales J. Graphitized carbons of variable morphology and crystallinity: A comparative study of their performance in lithium cells. . J Electrochem Soc 2009; 156:A986-A992.

[27] Bruce PG, Scrosati B, Tarascon JM. Nanomaterials for rechargeable lithium batteries. Angew Chem 2008; 47:2930-2946.

[28] Aurbach D, Teller H, Levi E. Morphology/behavior relationship in reversible electrochemical lithium insertion into graphitic materials. J Electrochem Soc 149; 2002:A1255-A1266.

[29] Wang X, Gai GS, Yang YF, Shen WC. Preparation of natural microcrystalline graphite with high spherecity and narrow size distribution. Powder Technol 2008; 181:51-56.

[30] Wu XL, Liu Q, Guo YG, Son WG. Superior storage performance of carbon nanosprings as anode materials for lithium-ion batteries. Electrochem Commun 2008; 11:1468-1471.

[31] Zaghib K, Song X, Guerfi A, Kostecki R, Kinoshita K. Effect of particle morphology on lithium intercalation rates in natural graphite. J Power Sources 2003; 124:505-512.

[32] Spahr ME, Wilhelm H, Palladino T, Dupont-Pavlovsky N, Goers D, Joho F, et al. The role of graphite surface group on graphite exfoliation during electrochemical lithium insertion. J Power Sources 2003; 119-121:543-549.

[33] Béguin F, Chevallier F, Vix-Guterl C, Saadallah S, Bertagna V, Rouzaud JN, et al. Correlation of the irreversible lithium capacity with the active area of modified carbons. Carbon 2005; 43:2160-2167.

[34] Novák P, Ufheil J, Buqa H, Krumeich F, Spahr ME, Goers D, et al. The importance of the active surface area of graphite materials in the first lithium intercalation. J Power Sources 2007; 174: 1082-1085.

[35] Guerin K, Fevrier-Bouvier A, Flandris S, Couzi M, Simon B, Biensan P. Effect of graphite crystal structure on lithium electrochemical intercalation. J Electrochem Soc 199; 146:3660-3665.

[36] Aurbach D, Teller H, Kolypin M, Levi E. On the behaviour of different types of graphite anodes. J Power Sources 2003; 119-121:2-7.

[37] Winter M, Novák P, Monnier J. Graphites for lithium ion cells. The correlation of the first cycle charge loss with the Brunauer-Emmett-Teller surface area. J Electrochem Soc1998; 145:428-436.